BOLETIN DE LA SOCIEDAD ESPAÑOLA DE
Cerámica y Vidrio
www.elsevier.es/bsecv

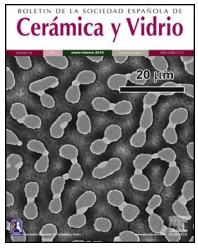

Original

Kinetic study on the effect of adding P_2O_5 to the LMAS glass-ceramic

Khalissa Ariane[a], *Aitana Tamayo*[b,*], *Abdellah Chorfa*[a,c], *Fausto Rubio*[b], *Juan Rubio*[b]

[a] *Institute of Optics and Precision Mechanics, Ferhat Abbas University Setif 1, Setif, Algeria*
[b] *Instituto de Cerámica y Vidrio, CSIC, Madrid, Spain*
[c] *Laboratory of Applied Optics, IOMP, Ferhat Abbas University Setif 1, Setif, Algeria*

ARTICLE INFO

Article history:
Received 13 August 2019
Accepted 22 November 2019
Available online 19 December 2019

Keywords:
LMAS glass-ceramic
Glass stability
Crystallization mechanism
A/L ratio
P_2O_5 effect

ABSTRACT

Glasses in the LMAS (Li_2O, MgO, Al_2O_3, SiO_2) system containing F, CaO, ZrO_2, and TiO_2 were subjected to crystallization by incorporating P_2O_5. The glass stability, glass forming ability, and crystallization kinetics have been determined. Crystals of Lithium Aluminum Silicate ($Li_xAl_xSi_{1-x}O_2$), Enstatite ($MgSi_2O_6$) and β-spodumene ($LiAlSi_2O_6$) were detected in the samples containing F, but β-spodumene was not observed in the glass-ceramic in its absence. Glasses containing F show a dependence of the activation with the addition of P_2O_5 with energy values ranging from 426 kJ mol^{-1} to 483 kJ mol^{-1}, being this maximum found for P_2O_5 amounts up to 3 mol%. High concentrations of P_2O_5 and Al_2O_3 improve the glass stability and increase the crystallization temperature. The most common crystallization mechanism is of bulk type with a constant number of nuclei. Two- and three-dimensional growth of crystals was observed in glasses containing F but in its absence and at high Al_2O_3 concentration bulk crystallization with two- and one-dimensional growth is observed.

Estudio cinético sobre el efecto de agregar P_2O_5 a la vitrocerámica LMAS

Palabras clave:
Vitrocerámico LMAS
Estabilidad vítrea
Mecanismo de cristalización
Relación A/L
Efecto P_2O_5

RESUMEN

Vidrios del sistema LMAS (Li_2O, MgO, Al_2O_3, SiO_2) y que contienen además F, Ca, ZrO_2 y TiO_2 han sido llevados a cristalización mediante la adición de P_2O_5. La estabilidad vítrea, capacidad formadora de vidrio y cinética de cristalización han sido estudiadas. Se ha determinado la presencia de cristales de aluminosilicato de litio ($Li_xAl_xSi_{1-x}O_2$), enstatita ($MgSi_2O_6$) y β-espodumena ($LiAlSi_2O_6$) en los vidrios que contenían F; sin embargo, sin la presencia de este, no se ha podido detectar β-espodumena. Los vidrios que contenían F muestran una dependencia en la energía de activación con el contenido en P_2O_5, encontrándose valores que oscilaban entre 426 kJ/mol y 483 kJ/mol, este último, el máximo encontrado para contenidos en P_2O_5 de hasta un 3%. A altas concentraciones de P_2O_5 y Al_2O_3 se observó un

* *Corresponding author.*
E-mail address: aitanath@icv.csic.es (A. Tamayo).
https://doi.org/10.1016/j.bsecv.2019.11.003

aumento de la estabilidad vítrea y de la temperatura de crista-lización. Durante la cristalización, el mecanismo más común observado es una cristalización masiva con un número constante de núcleos. Se observó un crecimiento en dos y tres dimensiones en los cristales que contenían F, pero en aquellos preparados sin F y a altas concentraciones de Al_2O_3, la cristalización masiva con crecimiento uni- y bidimensional se apreció preferentemente.

Introduction

During last decades, increasing interest in glass ceramic materials (GCM) has been developed in both scientific and technological point of view. These materials present interesting properties such as low thermal expansion coefficient, thermal and chemical stabilities even at high temperatures, biocompatibility, good mechanical resistance, etc. [1,2]. In the technological aspect, GCM are used in conventional or advanced technology fields such as healthcare (dental restoration [3], bone tissue regeneration [4]), domestic uses (glazes for ceramic tiles [5] or digital ceramic inks [6]), armors [7], telecommunications [8], energy generation [9], optical systems [10,11], electronics [12], etc. Up to now, most of the scientific literature is focused in research on the nucleation and crystallization processes as a function of the additives (F, P_2O_5, TiO_2, ZrO_2, etc.) [13], thermal schedule [14] or preparation processes [14–16].

GCM cover a vast family of materials which can be prepared with a wide range of chemical compositions depending on their final use [17]. Among all the different systems, Li_2O–SiO_2 (LS) [18], Li_2O–Al_2O_3–SiO_2 (LAS) [19], MgO–Al_2O_3–SiO_2 (MAS) [20] and CaO–MgO–Al_2O_3–SiO_2 (CMAS) [21] are the most widely studied. LS glass ceramics are applied for dental applications due to their interlocked microstructure [2], whereas LAS glass ceramics present excellent thermal shock resistance and low coefficient of thermal expansion (CTE) which in association with their high transparency broadly open their application fields [2]. The good mechanical properties of MAS glass ceramics (because of the crystallization of cordierite and sapphirine) make these materials excellent candidates in conventional and top technologies involving microwave radiation [22,23]. Some other compositions, such the CAS glass ceramics are mostly studied as low temperature co-fired ceramics (LTCC) [24] whereas CMAS glass ceramics can be used as sealants for solid oxide fuel cells [25].

Despite all those possibilities, the majority of GCM systems are mainly based on two or three oxides of the type of SiO_2, Li_2O, Al_2O_3, MgO and CaO. However, during last years more complex systems like LMAS and CMAS are gaining scientific and technological interest. In the case of the LMAS system, the approach is based in substituting a given concentration of the Li_2CO_3 expensive raw material for less expensive oxides and minerals, reaching Li_2O/MgO (*L*/*M*) ratios varying from 0.02 to 137.5 [26]. Other different oxides like Na_2O, K_2O, CaO, B_2O_3 and ZnO can form part of the LMAS system thus rendering different properties. At the same time, different nucleating agents are normally employed being TiO_2, ZrO_2, F and P_2O_5 the most frequently used to increase the crystalline phases in this LMAS and other GCM systems. The use of a mixture of the TiO_2, ZrO_2 and F nucleating agents in the same GCM has demonstrated to present a synergistic effect on the crystallization mechanism of spodumene–willemite–diopside glasses [27]. Similarly, the use of more complex nucleating agents provides important effects in the crystallization and microstructure of CMAS glass-ceramic materials [25]. Due to the complexity in the study of the crystallization mechanisms attributed to the use of these complex nucleating agents in the LMAS system, they have been rarely studied and in the few reports found in the literature, such agents are used in very low concentrations [26,28]. The challenge reported in this work is to achieve a detailed knowledge on the effect of both Al_2O_3 and P_2O_5 amounts on the crystallization kinetics of LMAS materials in the presence and in the absence of fluorine as nucleating agent.

Experimental procedure

Samples preparation

The starting raw materials were SiO_2 (purity >99.0%), Al_2O_3 (purity >99.5%), TiO_2 (purity 99.9%), P_2O_5 (purity >98.0%), $MgCO_3$ (purity >99.5%), Na_2CO_3 (purity >99.7%), cryolite (Na_3AlF_6, purity 98.5%), zirconium silicate ($ZrSiO_4$, purity 98.5%), $CaCO_3$ (purity >99.5%) and Li_2CO_3 (purity >99.8%). All of them were in the form of fine powders and mixed in different batches of 100 g. Then, they were calcined in a platinum crucible at 900 °C for 2 h and melted in an electric furnace at 1600 °C for 3 h in air atmosphere. The homogeneous melts were poured onto a preheated metallic plate and allowed to cool to room temperature. To ensure a good homogeneity, the obtained glasses were ground and melted again for 2 h. The obtained glasses were annealed immediately at 575 °C for 4 h and slowly left cool into the furnace to minimize thermal residual stresses. Three glasses were prepared with similar compositions (SiO_2, Al_2O_3, F, etc.) and increasing P_2O_5 concentration and, an additional glass was prepared without both P_2O_5 and F in order to analyze the effect of these nucleating agents in the crystallization mechanism.

Methods of characterization

The chemical compositions of the obtained glasses were determined using an X-ray fluorescence instrument with the analysis curve IQ+ (XRF, Philips, Magic Pro, USA). Crystallization kinetic parameters were analyzed by differential thermal analysis (DTA, TA Instruments, SDT Q600, USA) using glass powders sieved below 50 μm and heated from 25 to 1300 °C at

Table 1 – Chemical compositions (mol%) of the prepared glasses ($A/L = Al_2O_3/Li_2O$).

	Li_2O	MgO	Al_2O_3	SiO_2	CaO	Na_2O	TiO_2	ZrO_2	F	P_2O_5	A/L
0P-5A-F	10.95	15.16	5.32	58.21	0.34	1.51	5.40	2.20	0.86	0.00	0.48
1P-5A-F	11.28	15.00	5.31	57.41	0.33	1.82	5.37	2.13	0.49	0.81	0.47
3P-5A-F	11.91	14.71	5.20	55.42	0.34	1.52	5.15	2.07	0.51	3.12	0.44
2P-16A	9.28	13.40	16.38	50.56	0.30	1.39	4.79	1.98	0.00	1.87	1.76

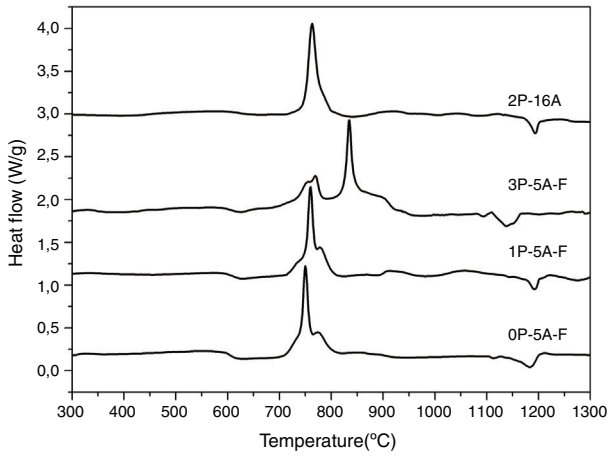

Fig. 1 – DTA curves of the LMAS glasses at the heating rate of 10 °C min^{-1}.

different heating rates (2, 5, 10 and 20 °C min^{-1}) in air atmosphere. Triplicated experiments were performed in series to determine the error in the characteristic temperatures. The glasses were crushed and sieved to different particle sizes (50–100, 100–200, 200–500 and 500–1000 μm) and an analyzed at 10 °C min^{-1} to estimate the dimensionality growth mechanism at each particle size. Pt crucibles filled with 50 mg glass sample were used. After crystallization, the developed crystalline phases were examined by X-ray diffraction (XRD, D8 Advance, Bruker Corp., Germany). The morphology of these crystalline phases was examined by field emission scanning electron microscopy (FE-SEM, Hitachi 4700, Japan) operating at 20 kV and backscattered electrons. Fractured surfaces were etched with a 3% HF solution for 15 s, rinsed with deionized water until removed all HF and then dried at 50 °C before observation in the FE-SEM.

Results and discussion

The obtained glasses were all transparent with a yellowish tonality for low P_2O_5 concentration that turns to brown for the high P_2O_5 content. The experimental chemical compositions of these glasses as analyzed by XRF are given in Table 1.

Fig. 1 shows the DTA thermograms of the obtained glasses. All the DTA curves exhibit similar trends with a small endothermic signal around 600 °C corresponding to the glass transition temperature, T_g. The observed exothermic peaks, labeled T_p in Fig. 1 correspond to the formation of the different crystalline phases. In the temperature range comprised between 1100 and 1300 °C, another endothermic signal is also detected and correspond to the melting point, T_m, of the crystals. In regard to the crystallization peaks, it should be noticed that all the samples show the principal peak whose position depends on the chemical composition of the glass. However, for the fluorine containing glasses and those produced with no or with low amounts of P_2O_5, the main exothermic peak is shown like centered between two small reflections, assigned to pre-nucleation events [29]. When a high P_2O_5 amount is added, the main peak appears at higher temperature than the two small ones. The described results are perfectly related with the well recognized effect of P_2O_5 as a crystallization promoter. In the case of the glass without F, the main crystallization peak appears before and at the lowest temperature and just one small right-hand shoulder accompaines this transition.

In Fig. 2 it is presented the DTA curves of each glass heated at different rates where we have highlighted the temperature range where the crystallization peaks are observed. The precise crystallization temperatures have been determined by curve fitting deconvolution, assuming that every peak presents a mixed Gaussian–Lorentzian (50–50%) shape. From these fitted peak, the exact positions (temperatures), full-widths (Δw) and intensities are obtained. Table 2 collects the temperatures labeled T_g and T_p and those corresponding to the onset of crystallization, T_0.

From the results presented in Tables 1 and 2, it can be deduced that when the F nucleant agent is not added into the glass composition, just one peak, sometimes accompained with a small shoulder, appear in the DTA (sample 2P-16A). However, in the presence of F, the thermograms show at least three peaks whose definition is increased because of the addition of both P_2O_5 and F. Data of Table 2 also show that T_g and T_p increase with the P_2O_5 content. These results are in line with several works that correlate the increase of T_g and T_p with the addition of P_2O_5 [30,31] or both F and P_2O_5 [32] to MAS and LAS glasses, respectively. In the literature, it is also described that if the concentration of Li_2O is higher than MgO, the addition of either P_2O_5 or F leads to a decrease of T_g and T_p [28,32,33]. T_g and T_p temperatures are indications of the tendency to maintain the glass structure or crystallize.

According to Table 2, the A/L ratio influences T_g and T_p in the sense that if this ratio is less and close to 0.2, the P_2O_5 acts as a nucleation promoter leading to a decrease of T_g and T_p; by if such ratio is higher than 0.7 P_2O_5 acts as glass stabilizer increasing these characteristic temperatures [34]. Results in Table 2 show that $A/L \geq 0.2$ for all the studied glasses and the effect of a the addition of P_2O_5 induce a stabilization of the glass network.

An exahustive exploration of the different regions in the DTA curves was also carried out in the next sections to analyze the crystallization mechanism of the LMAS glass-ceramics. In the first region, T_g informs about the structural relaxation occurring in the glass network when the material is subjected to a heating process. In this region the glass structure is

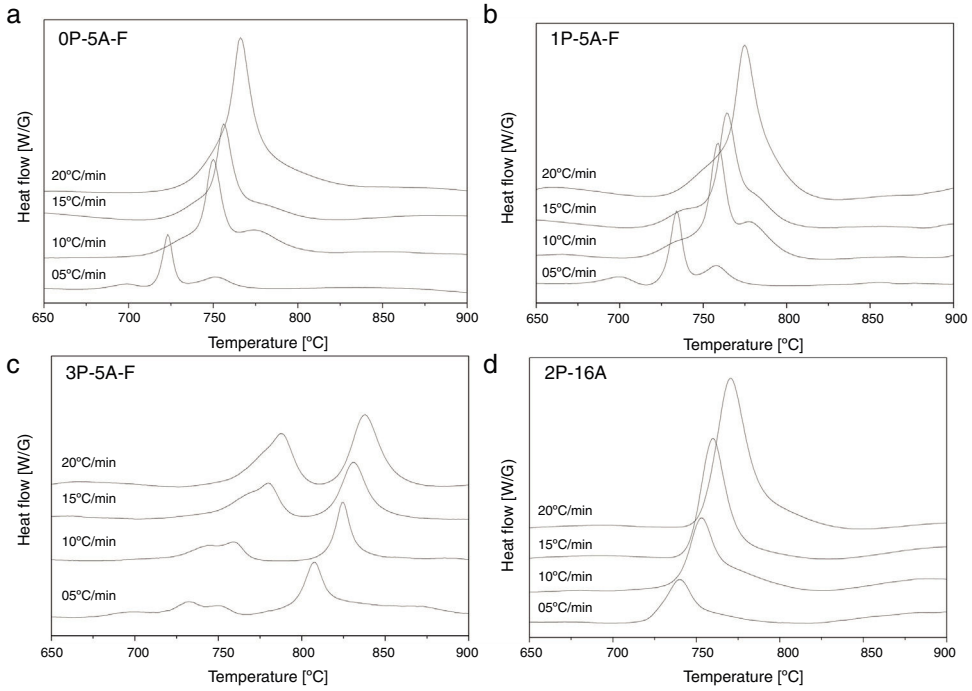

Fig. 2 – DTA curves of the LMAS glasses at different heating rates.

Table 2 – Characteristic temperatures (°C) from the DTA curves (the error in the determination of T_g, T_0, T_p and T_m is estimated to be ±2 °C).

Sample	Heating rate [°C min^{-1}]	T_g	T_0	T_{p1}	T_{p2}	T_{p3}	T_m
0P-5A-F	05	607	680	697	723	751	1200
	10	615	682	733	750	777	1201
	15	619	683	741	756	780	1202
	20	628	684	752	766	789	1202
1P-5A-F	05	616	660	699	734	758	1201
	10	624	688	735	759	778	1202
	15	629	690	737	764	782	1023
	20	635	695	754	775	789	1203
3P-5A-F	05	619	658	733	751	808	1165
	10	625	696	746	760	825	1166
	15	635	705	771	781	832	1168
	20	640	719	781	789	838	1169
2P-16A	05	624	715	740	763		1202
	10	628	734	753	778		1204
	15	635	735	760	788		1205
	20	644	741	770	794		1206

relaxed from internal tensions and molecular motion within the glass matrix may occur. The second region corresponds to the temperatures between T_g and T_p and/or T_m. By using these characteristic temperatures, it is possible to obtain information about the glass forming ability and glass stability and the tendency to crystallization of the glass network. Finally, the third region is where T_p appear and informs about the crystallization kinetics of the glass.

Structural relaxation and fragility index (F_I)

The F_I index was firstly proposed by Angell for characterizing the structural relaxation ocurring in a glass network when is heated below its T_g [35]. If the glass presents a resistance to a structural relaxation, it is referred as *strong glass*, but if such resistance is small it is described a *fragile glass*. These differences appear if T_g values present an Arrhenius temperature dependence with the viscosity. It is commonly accepted that an Arrhenius temperature dependence with its viscosity is exhibited by the so-called strong glasses.

This index, F_I, is considered a kinetic property since it is related to the variation of the glass viscosity near T_g so the determination of, F_I must be ideally performed through viscosity measurements. Nevertheless, these type of measurements are in general extremely difficult when the inorganic glasses present strong crystallization tendencies or high melting temperatures [36]. An elegant approach to overcome this issue is the employment of indirect methods based in differential

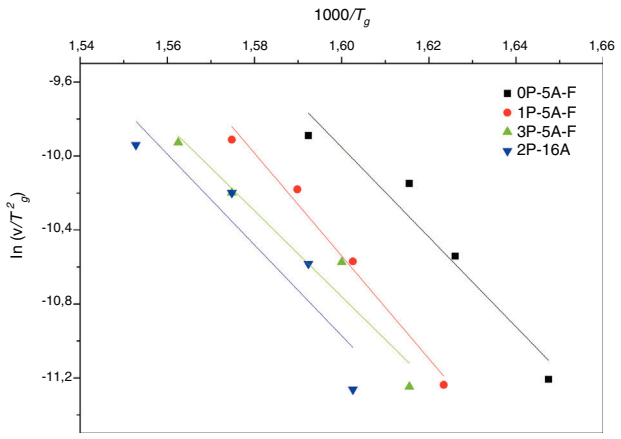

Fig. 3 – $\ln(v/T_g^2)$ vs $1000/T_g$ plots and activation energies of viscoglass in the different glasses transition range.

thermal analyses [37–39]. Among these methods, probably the most used one is the Kissinger method that can be expressed as in equation [38]:

$$\ln\left(\frac{T_g^2}{v}\right) = \frac{E_g}{RT_g} + C \quad (1)$$

where v is the DTA heating rate, E_g is the activation energy of glass transition which takes into account the molecular motion and rearrangement of atoms around T_g, R is the universal gas constant and C is also a constant.

The F_I index calculated from the DTA measurements ($F_{I\text{-}DTA}$) can now be expressed as a function of both E_g and T_g according to [40,41]:

$$F_{I\text{-}DTA} = \frac{E_g}{RT_g \ln 10} \quad (2)$$

The reported values of F_I varies widely within the range comprised between $F_I = 14.97$ for *strong glasses* and $F_I = 200$ for *fragile glasses* [42]. It should be advised there that the use of Eq. (1) together with the DTA data instead of using the viscosity measurements could lead in some errors in the determination of the correct F_I values. However, Zheng et al. [43] demonstrated that the differences between the T_g values as obtained by either one or the other technique are completely equivalents just by taking into account that the T_g data obtained by DTA can be used if the following equation is employed:

$$F_{I\text{-}vis} = 1.289(F_{I\text{-}DTA} - F_{I-0}) + F_{I-0} \quad (3)$$

where $F_{I\text{-}vis}$ is the correct fragility ($F_I = F_{I\text{-}vis}$) determined from viscosity measurements and $F_{I\text{-}0}$ is the reference fragility corresponding to a pefect strong glass which exhibits an Arrhenius behavior ($F_{I\text{-}0} = 14.97$).

The calculation of the E_g values from Eq. (1) is carried out by fitting the data shown in Fig. 3 to a straight line, being the results collected in Table 3. E_g values are in the range of silicate glasses with an Al_2O_3 molar concentrations varying between 0% and 20% [43,44]. From the calculated E_g values, the $F_{I\text{-}DTA}$ and $F_{I\text{-}vis}$ indexes are obtained by using Eqs. (2) and (3). As observed in Table 3, the F_I values of the studied glasses are higher than the values reported for vitreous silica which is close to 19 [36,45]. As observed in Table 3, the higher the E_g the higher F_I, and also, the obtained glasses can be considered as *strong glasses* since all F_I values are higher than the silica glass ($F_I = 19$).

It is also observed that E_g and F_I increase only with the addition of a small amount of P_2O_5 (0.81 mol%) to the glass composition but if more P_2O_5 is added E_g and F_I decrease. Variations of E_g and F_I can be explained on the basis of structural changes due to the introduction of phosphorus atoms. Although P_2O_5 generally acts as a nucleation agent to induce crystallization in silicoaluminate glasses containing Li, Mg, etc., it is also known that such effect strongly depends upon the A/L ratio [34]. For $A/L < 0.2$, P_2O_5 acts as a nucleating agent leading to an easy bulk crystallization and therefore the glass tends to be fragile whereas, if $A/L > 0.7$ P_2O_5 acts as a glass structure stabilizer improving the rigidity of the glass network, i.e. leading to a stronger glass. According to the chemical compositions provided in Table 2 and results of Tables 3 and 4, the studied glasses containing F present A/L ratios between 0.2 and 0.7 but they can be considered as strong glasses because their F_I values are closer to 19 than to 200. However, these results present some discrepancies because of the random variation with the P_2O_2 and Al_2O_3 content in the glasses. In order to discern these variations, the glass stability parameters are then further considered.

Glass forming ability and glass stability

The glass forming ability (GFA) is a parameter that indicates the facility of a melt to form a glass when is cooled and, therefore, it expresses the stability of a glass and its resistance to crystallization during cooling. At the same time, the glass stability (GS) expresses the resistance to crystallization when a cooled glass is heat-treated at increasing temperatures [35]. While GFA is related to melt glass cooling, GS is related to solid glass heating; although both parameters are related concepts, they are not equivalent [46] and present a strong correlation [47]. To study these parameters, we will use the region of the DTA curve between T_g and T_m. If the glass tends to devitrificate upon heating, new crystallization peaks will appear so, this region will provide the most valuable information about the glass stability.

In the literature, there are several equations that can be used for calculating GFA which principally differ in the use two or three characteristic temperatures of the DTA curve. Moreover, different works aimed to determine what are the best approaches, but the general conclusion is that it is not possible to select only one equation that would be valid for all glass materials, although it seems that those equations that use three characteristic points present higher correlation with GFA. In this sense, we have selected the equations described by Zhang et al. [48] and Yuan et al. [49] who defined the parameters ω_2 and β (Eqs. (4) and (5), respectively) because in most of the analysis they have shown much more sensitivity to changes in T_0/T_g and T_m/T_g temperature ratios:

$$\omega_2 = \frac{T_g}{2T_0 - T_g} - \frac{T_g}{T_l} \quad (4)$$

Table 3 – GS and GFA parameters ($F_{I\text{-}vis}$ calculated form Eq. (3), ω_2, β, K_H and S calculated as an average for the four heating rates).

	E_g (kJ mol^{-1})	$F_{I\text{-}DTA}$	$F_{I\text{-}vis}$	ω_2	β	K_H	S
0P-5A-F	426	25.03	27.94	0.27	3.14	0.12	3.46
1P-5A-F	483	28.10	31.89	0.27	3.26	0.12	2.98
3P-5A-F	403	23.33	25.75	0.25	3.95	0.14	4.42
2P-16A	424	24.48	26.23	0.21	4.07	0.21	2.65

Table 4 – Activation energies (kJ mol^{-1}) of each exothermic peak (Pk) for the studied glasses.

	0P-5A-F			1P-5A-F			3P-5A-F			2P-16A	
	Pk1	Pk2	Pk3	Pk1	Pk2	Pk3	Pk1	Pk2	Pk3	Pk1	Pk2
Kissinger	190	258	303	192	282	379	239	313	375	352	386
Ozawa	196	262	305	198	285	377	244	314	374	356	358
Augis and Bennett	199	252	316	204	284	388	256	332	395	374	381
Matusita and Sakka	195	285	422	180	342	336	221	319	431	378	342

$$\beta = \frac{T_0 T_g}{(T_l - T_0)^2} \tag{5}$$

where T_0 and T_l are the onset crystallization and liquidus temperatures, respectively.

Similarly, GS is mainly related to the differences between T_g and T_p and, although several equations have been proposed, Marques and Cabral [50] have shown that all of them can be used to accurate determine the GS in different glasses. One of these methods in that proposed by Hruby which, besides T_g and T_p it takes also into account T_m [51]. The Hruby parameter, K_H, is defined as:

$$K_H = \frac{T_0 - T_g}{T_m - T_0} \tag{6}$$

where T_m is the melting temperature. When using the Hruby equation, it is considered that GS increases with K_H. Similarly, another equation proposed by Saad and Poulain (S) reflected the resistance to devitrification of a glass when it's heated [52]:

$$S = \frac{(T_p - T_0)(T_0 - T_g)}{T_g} \tag{7}$$

In Table 3 we have collected the ω_2, β, K_H and S values obtained for the LMAS glasses studied in this work and calculated as the averaged value for the four heating rates.

According to Marques and Cabral [50], some GS parameters are well correlated to the GFA, nevertheless they can express a different behavior: some of them, β, K_H and S are directly proportional to the GFA, while ω_2 is inversely proportional to GFA. The results recorded in Table 3 show that the addition of P_2O_5 to the LMAS glasses leads to an increase in β, K_H and a decrease in ω_2, which is translated is an increase in the GFA and GS of the glasses. The absence of F and the higher Al_2O_3 content in the 2P-16A glass confers to this glass the major stability.

It is also noticed that the S values do not follow any trend like the other three parameters so we cannot extract any correlation or conclusion. This problem may arise because the S parameter takes into account both the T_p values and the corresponding differences between T_p and T_0, and the studied glasses present several crystallization peaks so, it is difficult to analyze. Since at low heating rates, the peaks are mostly well ressolved, we performed these calculations by solely using T_{p2} values of Table 2 at the 5 °C min^{-1} heating rate, being 3.66, 3.70, 4.07 and 4.87 the obtained S values for the 0P-5A-F, 1P-5A-F, 3P-5A-F and 2P-16 glasses, respectively. This is then translated as an increase in GS like the other parameters have shown. We think that the behavior of the S parameter still needs a toughtful study for the different glasses and also in a wider range of compositions where several crystallization peaks appear.

Crystallization kinetic mechanism

The DTA curves have been used to determine the crystallization mechanisms and the activation energies (E_c) for crystal growth through the analysis of the exothermic peaks at different heating rates. All kinetic analysis models of non-isothermal DTA data are based on the Johnson–Mehl–Avrami–Kolmogorov relation (JMAK):

$$x = 1 - \exp(-NU^m t^n) \tag{8}$$

where x is the crystallized fraction volume, N is related to the number density of nuclei with a crystalline phase factor, U is the growth rate, m is the growth morphology index, which depends on the dimensionality of the crystal growth, t is the time and n is the Avrami exponent. In most of cases $m = n$ and then Eq. (8) can be written as Eq. (9)

$$x = 1 - \exp(-(At)^n) \tag{9}$$

where n now depends on both the growth mechanism and the dimensionality of the crystal and A is the Arrhenian pre-exponential factor depending on the temperature:

$$A = A_0 \exp\left(-\frac{E_c}{RT_c}\right) \tag{10}$$

where A_0 is the frequency factor and E_c is the activation energy for the whole process, i.e. it takes into account the nucleation and growth processes and, in some cases the activation energies of different crystalline phases crystallizing at similar temperatures.

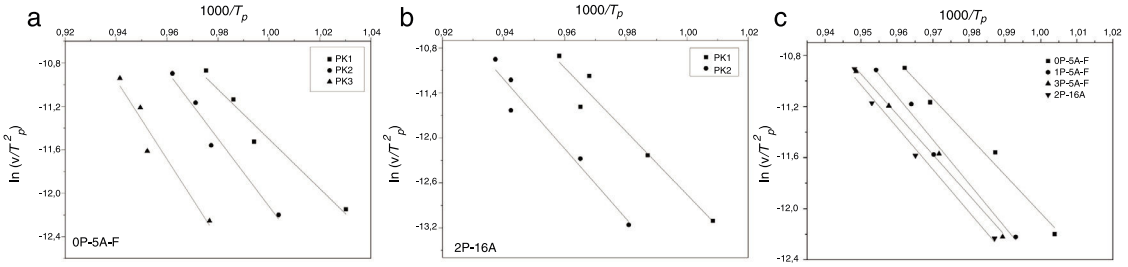

Fig. 4 – Kissinger plot ($\ln(v/T_p^2)$ vs $1000/T_p$ plot): 0P-5A-F (a), 2P-16A (b) and (c) for all different glasses at the temperature of main peak.

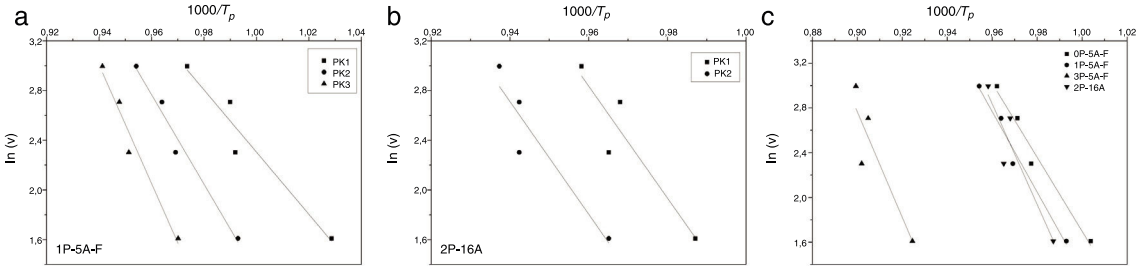

Fig. 5 – $\ln(v)$ vs $1000/T_p$: (a) for 1P-5A-F, (b) for 2P-16A and (c) for temperature of main peak of the different glasses.

The parameters m and n can take various values: for surface crystallization $n=m=1$, for bulk crystallization with a constant number of nuclei independent of temperature $n=m$ and, for bulk crystallization with an increasing number of nuclei inversely proportional to the heating rate $n=m+1$ [53]. In these later cases of bulk crystallization m can take values of 3, 2 or 1 if the dominating growth mechanism of the crystals is three-dimensional, two-dimensional or one-dimensional, respectively.

In order to determine the activation energies for crystallization and the corresponding mechanism, the first kinetics model we are using was developed Kissinger [38,54] who established that the activation energy, E_{ck}, can be obtained from the heating rate dependence of the crystallization peak temperature according to the equation:

$$\ln\left(\frac{v}{T_p^2}\right) = \frac{-E_{ck}}{RT_p} + \text{cte} \tag{11}$$

where v is the DTA heating rate. Kissinger plots for the different studied glasses at heating rates of 5, 10, 15 and 20 °C min^{-1} are shown in Fig. 4, and the corresponding E_{ck} values are given in Table 4. As it has been mentioned before, the peak temperature has been determined by deconvoluting the DTA curve into two or three Gaussian peaks.

In a similar fashion, Ozawa [55,56] proposed a modified form of the Kissinger's equation. According to Ozawa model, the change of $\ln(1/T_p^2)$ with v is negligibly small compared to the change of $\ln(v)$ and therefore, the Kissinger's equation must be written as:

$$\ln(v) = -1.0516\frac{E_{co}}{RT_p} + \text{cte} \tag{12}$$

Fig. 5 shows $\ln(v)$ vs $1000/T_p$ plot and the value of E_{co} can be obtained from the slope of the straight line according to Eq. (12).

To further confirm the accuracy of the above results for activation energy values, Augis and Bennett [57] developed a more exact method for determining crystallization parameters:

$$\ln\left(\frac{v}{T_p - T_0}\right) = \frac{-E_{cab}}{RT_p} + \text{cte} \tag{13}$$

where the differences between T_p and T_0 are taken into account [58]. Fig. 6 shows the plot $\ln(v/(T_p - T_0))$ vs $1000/T_p$ from which the E_{cab} has been obtained.

Once the E_{cab} is known, the Augis and Bennett method [57] permits the determination of the Avrami parameter n:

$$n = \frac{2.5RT_p^2}{\Delta w\, E_{cab}} \tag{14}$$

where Δw is the full-width of the exothermic peak at half-maximum intensity. As evidenced in Eq. (13), higher Δw values result in smaller n values, and vice versa.

Matusita and Sakka [59] deduced that Eq. (11) was only valid if the crystal growth occurs over a fixed number of nuclei and suggested a modified form of the Kissinger equation which can be written as:

$$\ln\left(\frac{v^n}{T_p^2}\right) = -m\frac{E_{cms}}{RT_p} + \text{constant} \tag{15}$$

As it can be observed, this equation takes into consideration the two parameters, n and m, which characterize the crystallization growth mechanism and the activation energy. In Eq. (15), it is assumed that n and E_{cms} are constants for a given material but Marques et al. [60] have shown that n and E_c vary with the particle size. They also demonstrated that for

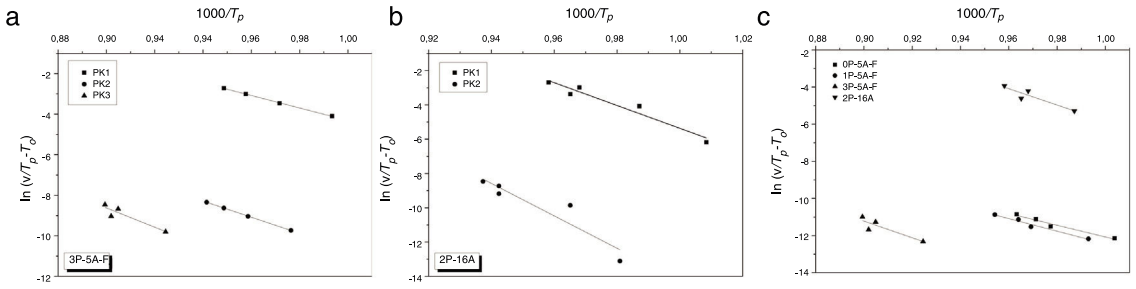

Fig. 6 – ln(v/(T_p – T_0)) vs 1000/T_p. 3P-5A-F (a), 2P-16A (b), and for the different glasses at the temperature of main peak (c).

Table 5 – *n* and *m* parameters for the studied glasses. Pk1, Pk2 and Pk3 indicate each one of the peaks detected in the thermograms.

		0P-5A-F			1P-5A-F			3P-5A-F			2P-16A	
		Pk1	Pk2	Pk3	Pk1	Pk2	Pk3	Pk1	Pk2	Pk3	Pk1	Pk2
Augis and Bennett	*n*	2.9	4.2	1.4	2.7	3.5	1.7	1.8	2.9	2.2	2.1	0.9
Matusita and Sakka	*m*	2.9	4.5	1.3	2.6	3.6	1.7	1.7	2.9	2.2	2.0	0.8

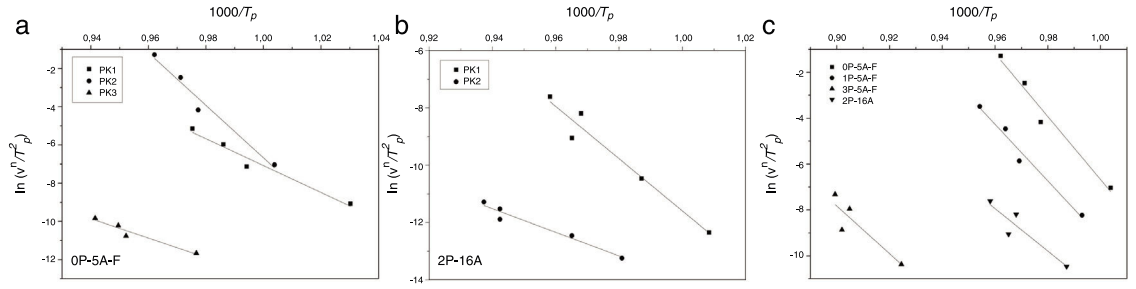

Fig. 7 – Plot of ln(v^n/T_p^2) vs 1000/T_p. 0P-5A-F (a), 2P-16A (b), and for the different glasses at the temperature of main peak (c).

small particles (<105 μm and 105–355 μm) both values present a little variations and, thus the above referred equation is suitable for our work since in all the cases, the particle size is maintained below 50 μm. The values of E_c for crystallization calculated by different methods, the values of Avrami exponent n and the m parameter are given in Tables 4 and 5 and Fig. 7.

In addition to that, Xu et al. [61] reported that for most oxide-glass systems E_c and E_{ck} are related through the equation:

$$E_c = \frac{n}{m} E_{ck} \tag{16}$$

Here, when $m = n$, crystallization occurs on a fixed number of nuclei and $E_{ck} = E_c$. Thus, for crystal growth that occurs on a fixed number of nuclei, the analysis of DTA data by the Kissinger model, Eq. (11) yields the correct value of E_c. When the number of nuclei changes during the DTA measurements, we have the option to use Eq. (14) or we can determine E_{ck} from Eq. (11) and then multiply this term by n/m to obtain the correct activation energy.

As mentioned before, the DTA curves present two or three peaks so, the E_c and n and m values can be calculated in each peak. The differences in the E_c values determined by different methods may be attributed to the different approximations that have been adopted while arriving at the final values from them, but, in most cases, the results are very close and the discussion of the crystallization kinetics can be carried out by taking the average values of each parameter. The activation energies of Table 4 are in the range of 200–400 kJ mol^{-1} as correspond to a LAS or MAS glass ceramic material [62]. From the data of Table 4 it is clear that for the glasses with 5% of Al_2O_3 E_c values increase with T_p indicating that it is necessary higher temperatures to induce crystal growth. However, in the glass with 16% of Al_2O_3 and although the two crystallization peaks appear at temperatures close to the low temperature peaks of the other glasses with lower Al_2O_3 concentration, the E_c values for such two crystallization peaks are very close the one of the high temperature peak of low Al_2O_3 glasses. We attribute this result to the effect of Al_2O_3 limiting the mobility of the crystal forming cations [63].

The effect of P_2O_5 on the crystallization kinetics of LAS and MAS glasses has been extensively studied [28,63,64]. P_2O_5 is considered as a crystallization promoter due to its nucleating role; however it has recently shown that such role depends on the composition of the parent glass. If K_2O and Al_2O_3 are replaced by P_2O_5, the activation energy for the crystallization decreases [63]. A similar effect that is observed if P_2O_5 is added to a glass with an A/L ratio lower than 0.4, however, if the A/L ratio is higher than 0.7 then P_2O_5 acts as a glass structure stabilizer due to the formation of POAl complexes that prevent the formation of the heterogeneities that inhibits glass

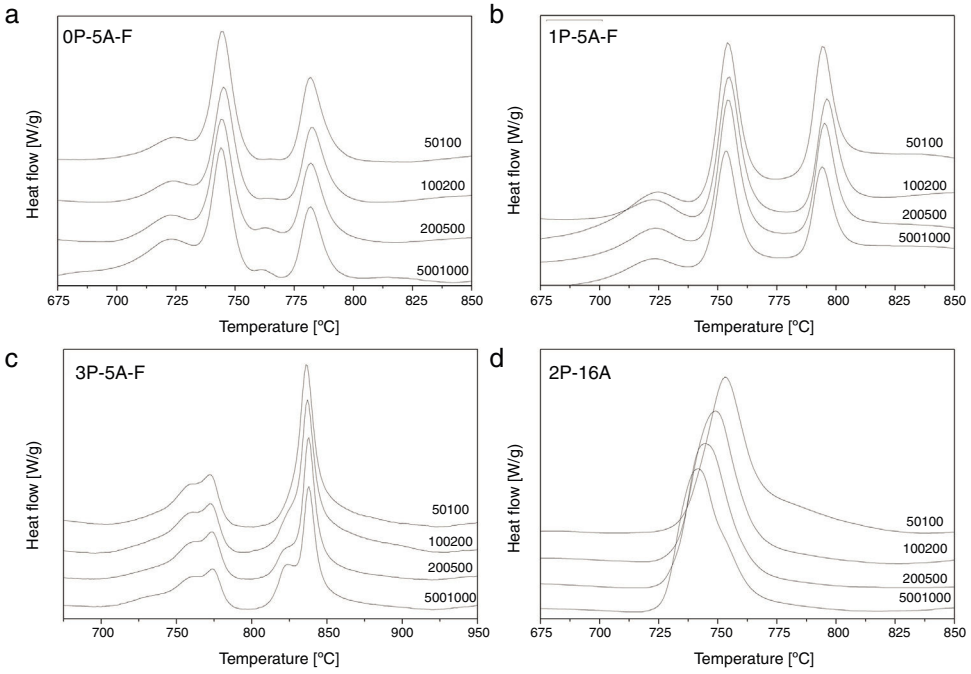

Fig. 8 – DTA plots of glass samples 0P-5A-F, 1P-5A-F, 2P-16A and 3P-5A-F for different particle sizes.

crystallization [34]. Results in Table 4 indicate that for the LMAS glasses containing 5% of Al_2O_3 (with Al/L around to 0.47) the addition of 1% and 3% of P_2O_5 leads to an increase in E_c, a result that indicates that P_2O_5 restrains the crystallization of the LMAS glass. Similarly, in the 2P-16A glass with $A/L = 1.76$, the high Al_2O_3 concentration and the addition of 2% of P_2O_5 also mitigates the glass crystallization and then the E_c values are the highest among all the studied glasses.

With respect to the *n* and *m* parameters, Table 5 shows that both parameters have the same values and, therefore, in accordance to Donald [53] and Matusita and Sakka [59] the crystallization mechanism is mainly of bulk type with a constant number of nuclei, although the specific values depends on the amount of F, P_2O_5 and Al_2O_3 in the glass. The main difference appears whit the presence of F and, it is observed that those glasses containing F present a different behavior than the one without it (2P-16A). For the F containing glasses the addition of P_2O_5 leads to a decrease of the *n* and *m* values for the first and second peaks, while for the third peak *n* and *m* increase. This result indicates that the incorporation of P_2O_5 leads to a homogeneous crystallization mechanism for the three peaks and mainly with two- and three-dimensional growth of crystals. On the other hand, for the 2P-16A glass without F the *n* and *m* values correspond to bulk crystallization with two- and one-dimensional growth of crystals.

In order to confirm the dimensionality growth mechanism, Ray and Day proposed a simple and rapid method to identify and distinguish surface from bulk crystallization [65]. This method consists on analyzing the T_p and $T_p^2/\Delta w$ as a function of the particle size. Because as particle size increases the surface to volume ratio decreases, if surface crystallization is the dominant mechanism, then T_p and $T_p^2/\Delta w$ will decrease and, on the contrary, for bulk crystallization they will increase. DTA plots for glass samples 0P-5A-F, 1P-5A-F, 3P-5A-F and

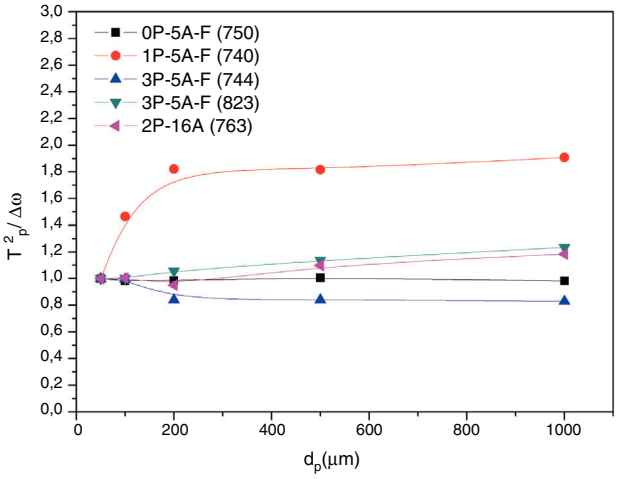

Fig. 9 – Plots of $T_p^2/\Delta w$ vs particle size for some peaks of glass samples.

2P-16A of different particle size (50–100, 100–200, 200–500 and 500–1000) are shown in Fig. 8. In all the glasses, it is observed the same crystallization peaks, but, in the case of the 0P-5A-F, 3P-5A-F glasses, a new peak appears at temperatures of 760 and 820 °C, respectively. The kinetic mechanism of this new peak was not subjected to the analysis described above but it is clear that it increases in intensity with the particle size indicating that the crystallization mechanisms is of bulk type. The rest of the crystallization peaks for these and other samples have been analyzed by the method described by Ray and Day. Fig. 9 presents the evolution of the $T_p^2/\Delta w$ for the main representative peaks of each glass. It is observed that the evolution of $T_p^2/\Delta w$ with the particle size varies from one glass to

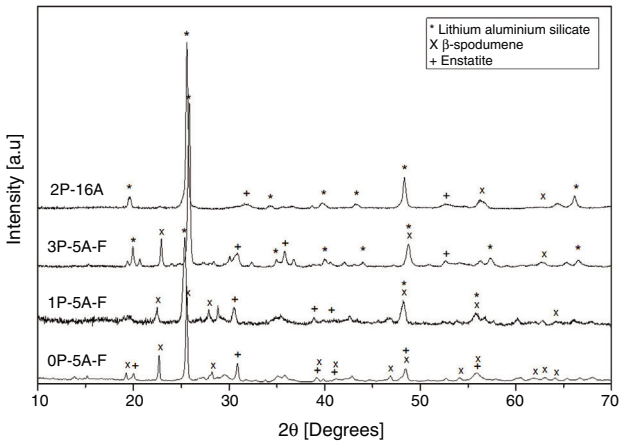

Fig. 10 – X-ray diffraction patterns of 0P-5A-F, 1P-5A-F, 2P-16A and 3P-5A-F heated at 860 °C.

another and, in the case of the 3P-5A-F that presents two main peaks both give different evolution. In this 3P-5A-F glass while the peak at 760 °C shows a decrease $T_p^2/\Delta w$ with the particle size, the one at 825 °C shows an increase. In general it could be said that the evolution of $T_p^2/\Delta w$ with the particle size is an appropriate method for obtaining a conclusion about the crystallization mechanism or for discriminating between surface and bulk crystallization types. This result has just been described by Marques et al. when analyzing the crystallization of lithium disilicate glasses [60].

XRD and microstructure analysis

Fig. 10 shows the XRD patterns for the different studied glass-ceramics after heat treating at 860 °C, i.e. when all the DTA peaks have appeared. In all cases, a high degree of crystallization is observed. As expected, the main signals are attributed to a Lithium Aluminum Silicate ($Li_xAl_xSi_{1-x}O_2$, JCPDS 00-040-0073), and some other small peaks attributed to Enstatite ($MgSi_2O_6$, JCPDS 00-022-0714) and β-spodumene ($LiAlSi_2O_6$, JCPDS 00-035-0797) also appeared in the samples containing F, i.e. 0P-5A-F, 1P-5A-F and 3P-5A-F. In all the cases and under identical experimental conditions, the intensity of the major diffraction peaks, $Li_xAl_xSi_{1-x}O_2$, increases with the P_2O_5 concentration, a result that indicates the influence of this nucleant agent in the crystallization reactions In the diffractogram of the sample 2P-16A without F and a high concentration of Al_2O_3 no traces of crystallization of β-spodumene was found. In accordance to these data, and from the results presented in Table 2 and Figs. 1 and 2, three exothermic crystallization peaks were found in the thermograms of the glasses with F which is in line with the three crystalline phases appearing in the XRD of Fig. 10. In the glass without F just two peaks were found in the thermogram and just two crystalline phases emerged in the XRD diffractograms. Thus, it must be assumed that each peak corresponds to a given crystalline phase. Further analysis of these results will be explored in a next work by using other characterization techniques such as Raman and IR spectroscopies.

SEM micrographs of the heat treated glasses are shown in Fig. 11. Here it is observed the presence some crystals with a globular shape. Similar results have been found in different works [26,66] that assigned the tiny globular particles to the $Li_xAl_xSi_{1-x}O_2$ crystals. It is observed that the sizes of these particles increase with the P_2O_5 content in the glass and reaching sizes higher than 500 nm. In the case of the 2P-16A glass ceramic (Fig. 11) the obtained microstructure is very similar to the one showed by Guo et al. [67] for a LAS glass-ceramic containing F, where the sizes were in the range of 50–100 nm. In all cases the crystallization is of bulk type, according to the *n* and *m* values of Table 5 and as it has been discussed throughout the work.

Conclusions

Several glasses in the LMAS (Li_2O, MgO, Al_2O_3, SiO_2) system with F, CaO, ZrO_2 and TiO_2 in their compositions have been prepared by melting at high temperatures. Glass stabilities and crystallization mechanisms have been analyzed by DTA as a function of P_2O_5 concentration and Al_2O_3/Li_2O ratio. These glasses crystallize in Lithium Aluminum Silicate ($Li_xAl_xSi_{1-x}O_2$), Enstatite ($MgSi_2O_6$) and β-spodumene ($LiAlSi_2O_6$) when F is in their composition, whereas β-spodumene does not appear if F is not present. These crystals appear as particles of globular shape whose sizes increase with the P_2O_5 content in the glass reaching values higher than 500 nm. The addition of F and P_2O_5 give an increase in the glass transformation and crystallization temperatures. Because the A/L ratio is higher than 0.2 in all cases the addition of P_2O_5 produces a stabilization of the glass network, a similar effect that appears if the glass presents a high Al_2O_3 concentration. The activation energies for crystallization are in the range of 400–500 kJ mol^{-1} as correspond to LAS and MAS glass ceramic materials. The obtained results indicate that for glasses containing 5% of Al_2O_3 (with Al/L around to 0.47) the addition of 1% and 3% of P_2O_5 lead to an increase in E_c, a result that indicates that in this study the P_2O_5 restrains the crystallization of the LMAS glass. In the case of the glass with A/L = 1.76 the high Al_2O_3 concentration and the addition of 2% of P_2O_5 mitigates

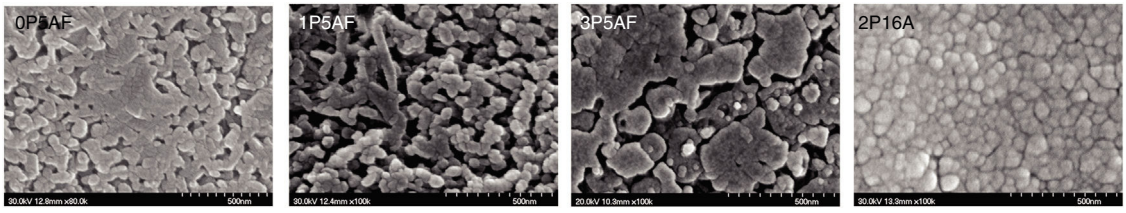

Fig. 11 – SEM micrographs of 0P-5A-F, 1P-5A-F, 3P-5A-F and 2P-16A, heat treated glass-ceramics at the main peak crystallization temperature, respectively.

the activation energy for glass crystallization. The incorporation of P_2O_5 or the high Al_2O_3 concentration increases the glass stability. The crystallization mechanism is mainly of bulk type with a constant number of nuclei, although and it depends on the amount of both Al_2O_3 and P_2O_5 in the glass. For the glass without F and high Al_2O_3 concentration the crystallization presents a one and two-dimensional growth of crystals, however for those glasses containing F the growth is two- and three-dimensional. The incorporation of P_2O_5 in the glass composition leads to a homogeneously crystallization mechanism.

Acknowledgements

The present work was supported by the Algerian Ministry of Higher Education and Scientific Research (Algerian program P.N.E 2016–2017 scholarship fund) and with the collaboration of the Institute of Ceramic and Glass ICV-CSIC, Madrid, Spain. This work was developed under the frame of the project MAT2016-78700-R.

REFERENCES

[1] P. James, Glass ceramics: new compositions and uses, J. Non-Cryst. Solids 181 (1995) 1–15.
[2] E.D. Zanotto, Bright future for glass-ceramics, Am. Ceram. Soc. Bull. 89 (2010) 19–27.
[3] M. Montazerian, E.D. Zanotto, Bioactive and inert dental glass-ceramics, J. Biomed. Mater. Res. Part A 105 (2017) 619–639.
[4] L.L. Hench, Opening paper 2015 – some comments on bioglass: four eras of discovery and development, Biomed. Glasses 1 (2015).
[5] C. Peng, M. Lv, C. Jing-Pei, C. Peng, M.J. Ding, J.Q. Wu, Cordierite glass-ceramic used for transparent tile glazes, J. Am. Ceram. Soc. 100 (2017) 4402–4406.
[6] J.W. Kwon, J.H. Lee, K.T. Hwang, J.H. Kim, K.S. Han, Formulation and evaluation of glass-ceramic ink for digital ink-jet printing, Korean J. Mater. Res. 27 (2017) 583–589.
[7] T. Benitez, S.Y. Gómez, A.P.N. de Oliveira, N. Travitzky, D. Hotza, Transparent ceramic and glass-ceramic materials for armor applications, Ceram. Int. 43 (2017) 13031–13046.
[8] S. Mitachi, R. Nagase, Y. Takeuchi, R. Honda, Durable glass ceramic ferrule for general telecommunication use, Glass Technol. 39 (1998) 98–99.
[9] C. Zhang, L. Wang, X. Ji, G. Li, G. Hou, Effect of melting times on the down-shifting properties in Ce^{3+}-doped oxyfluoride glass ceramics for a-Si solar cells, J. Russ. Laser Res. 38 (2017) 554–558.
[10] V. Khani, P. Alizadeh, M. Shakeri, Optical properties of transparent glass–ceramics containing lithium–mica nanocrystals: crystallization effect, Mater. Res. Bull. 48 (2013) 3579–3584.
[11] F.C. Serbena, G.P. Souza, E.D. Zanotto, J. Lumeau, L. Glebova, L.B. Glebov, Internal residual stresses in partially crystallized photo-thermo-refractive glass, J. Am. Ceram. Soc. 94 (2011) 671–674.
[12] M. Shakeri, M. Rezvani, Optical properties and structural evaluation of Li_2O–Al_2O_3–SiO_2–TiO_2 glassy semiconductor containing passive agent CeO_2, Spectrochim. Acta Part A: Mol. Biomol. Spectrosc. 83 (2011) 592–597.
[13] V. Maier, G. Müller, Mechanism of oxide nucleation in lithium aluminosilicate glass-ceramics, J. Am. Ceram. Soc. 70 (1987), C-176–C-178.
[14] M. Bengisu, R.K. Brow, Effect of long-term heating and thermal cycling on thermal expansion, phase distribution, and microhardness of lithium aluminosilicate glass-ceramics, J. Non-Cryst. Solids 331 (2003) 137–144.
[15] L.R. Pinckney, G.H. Beall, Microstructural evolution in some silicate glass–ceramics: a review, J. Am. Ceram. Soc. 91 (2008) 773–779.
[16] L. Xia, X. Wang, G. Wen, B. Zhong, L. Song, Nearly zero thermal expansion of β-spodumene glass ceramics prepared by sol–gel and hot pressing method, Ceram. Int. 38 (2012) 5315–5318.
[17] D.W. Richerson, The Magic of Ceramics, John Wiley & Sons, 2012.
[18] D. Holland, Y. Iqbal, P. James, B. Lee, Early stages of crystallisation of lithium disilicate glasses containing P_2O_5 – an NMR study, J. Non-Cryst. Solids 232 (1998) 140–146.
[19] E. Kleebusch, C. Patzig, M. Krause, Y. Hu, T. Höche, C. Rüssel, The formation of nanocrystalline ZrO_2 nuclei in a Li_2O–Al_2O_3–SiO_2 glass – a combined XANES and TEM study, Sci. Rep. 7 (2017) 10869.
[20] S. Reinsch, M.L.F. Nascimento, R. Müller, E.D. Zanotto, Crystal growth kinetics in cordierite and diopside glasses in wide temperature ranges, J. Non-Cryst. Solids 354 (2008) 5386–5394.
[21] Y. Shi, B.W. Li, M. Zhao, M.X. Zhang, Growth of diopside crystals in CMAS glass-ceramics using Cr_2O_3 as a nucleating agent, J. Am. Ceram. Soc. 101 (2018) 3968–3978.
[22] S.-B. Sohn, S.-Y. Choi, Y.-K. Lee, Controlled crystallization and characterization of cordierite glass-ceramics for magnetic memory disk substrate, J. Mater. Sci. 35 (2000) 4815–4821.
[23] L. Sant'Ana Gallo, F. Célarié, N. Audebrand, A.C. Martins Rodrigues, E.T. Dutra Zanotto, Rouxel, In situ crystallization and elastic properties of transparent MgO–Al_2O_3–SiO_2 glass-ceramic, J. Am. Ceram. Soc. 100 (2017) 2166–2175.
[24] S. Banijamali, B.E. Yekta, H. Rezaie, V. Marghussian, Crystallization and sintering characteristics of CaO–Al_2O_3–SiO_2 glasses in the presence of TiO_2, CaF_2 and ZrO_2, Thermochim. Acta 488 (2009) 60–65.
[25] X. Guo, X. Cai, J. Song, G. Yang, H. Yang, Crystallization and microstructure of CaO–MgO–Al_2O_3–SiO_2 glass–ceramics containing complex nucleation agents, J. Non-Cryst. Solids 405 (2014) 63–67.
[26] G. Xingzhong, Z. Lingjie, Y. Hui, Effects of Li replacement on the nucleation, crystallization and microstructure of Li_2O–Al_2O_3–SiO_2 glass, J. Non-Cryst. Solids 354 (2008) 4031–4036.
[27] A. El-Shennawi, A. Omar, A. Morsy, The role of titania and titania mixtures in the nucleation and crystallization of spodumene–willemite–diopside glasses, Thermochim. Acta 58 (1982) 125–153.
[28] X. Guo, H. Yang, C. Han, F. Song, Crystallization and microstructure of Li_2O–Al_2O_3–SiO_2 glass containing complex nucleating agent, Thermochim. Acta 444 (2006) 201–205.
[29] X. Guo, H. Yang, Effects of fluorine on crystallization, structure and performances of lithium aluminosilcate glass ceramic, Mater. Res. Bull. 41 (2006) 396–405.
[30] J.M. Wu, S.P. Hwang, Effects of (B_2O_3, P_2O_5) additives on microstructural development and phase-transformation kinetics of stoichiometric cordierite glasses, J. Am. Ceram. Soc. 83 (2000) 1259–1265.
[31] A. Arvind, A. Sarkar, V. Shrikhande, A. Tyagi, G. Kothiyal, The effect of TiO_2 addition on the crystallization and phase formation in lithium aluminum silicate (LAS) glasses nucleated by P_2O_5, J. Phys. Chem. Solids 69 (2008) 2622–2627.

[32] W. Zheng, J. Cui, L. Sheng, H. Chao, Z. Peng, C. Shen, Effect of complex nucleation agents on preparation and crystallization of CaO–MgO–Al_2O_3–SiO_2 glass-ceramics for float process, J. Non-Cryst. Solids 450 (2016) 6–11.
[33] W. Höland, E. Apel, C. van't Hoen, V. Rheinberger, Studies of crystal phase formations in high-strength lithium disilicate glass–ceramics, J. Non-Cryst. Solids 352 (2006) 4041–4050.
[34] P. Glatz, M. Comte, L. Cormier, L. Montagne, B. Doumert, G.G. Moore, Different roles of phosphorus in the nucleation of lithium aluminosilicate glasses, J. Non-Cryst. Solids 493 (2018) 48–56.
[35] C. Angell, Spectroscopy simulation and scattering, and the medium range order problem in glass, J. Non-Cryst. Solids 73 (1985) 1–17.
[36] Q. Zheng, J.C. Mauro, Y. Yue, Reconciling calorimetric and kinetic fragilities of glass-forming liquids, J. Non-Cryst. Solids 456 (2017) 95–100.
[37] C. Moynihan, S.-K. Lee, M. Tatsumisago, T. Minami, Estimation of activation energies for structural relaxation and viscous flow from DTA and DSC experiments, Thermochim. Acta 280 (1996) 153–162.
[38] H.E. Kissinger, Reaction kinetics in differential thermal analysis, Anal. Chem. 29 (1957) 1702–1706.
[39] L.-M. Wang, V. Velikov, C. Angell, Direct determination of kinetic fragility indices of glassforming liquids by differential scanning calorimetry: kinetic versus thermodynamic fragilities, J. Chem. Phys. 117 (2002) 10184–10192.
[40] K. Chebli, J. Saiter, J. Grenet, A. Hamou, G. Saffarini, Strong-fragile glass forming liquid concept applied to GeTe chalcogenide glasses, Physica B: Condens. Matter 304 (2001) 228–236.
[41] M. Wakkad, E.K. Shokr, S. Mohamed, Optical and calorimetric studies of Ge–Sb–Se glasses, J. Non-Cryst. Solids 265 (2000) 157–166.
[42] A. Goel, E. Shaaban, F. Melo, M. Ribeiro, J. Ferreira, Non-isothermal crystallization kinetic studies on MgO–Al_2O_3–SiO_2–TiO_2 glass, J. Non-Cryst. Solids 353 (2007) 2383–2391.
[43] Q. Zheng, M. Potuzak, J.C. Mauro, M.M. Smedskjaer, R.E. Youngman, Y. Yue, Composition–structure–property relationships in boroaluminosilicate glasses, J. Non-Cryst. Solids 358 (2012) 993–1002.
[44] W. Mi-Tang, C. Jin-Shu, Viscosity and thermal expansion of rare earth containing soda–lime–silicate glass, J. Alloys Compd. 504 (2010) 273–276.
[45] J.C. Mauro, Effect of fragility on relaxation of density fluctuations in glass, J. Non-Cryst. Solids 357 (2011) 3520–3523.
[46] M.C. Weinberg, Glass-forming ability and glass stability in simple systems, J. Non-Cryst. Solids 167 (1994) 81–88.
[47] A. Cabral, A. Cardoso, E. Zanotto, Glass-forming ability versus stability of silicate glasses. I. Experimental test, J. Non-Cryst. Solids 320 (2003) 1–8.
[48] P. Zhang, H. Wei, X. Wei, Z. Long, X. Su, Evaluation of glass-forming ability for bulk metallic glasses based on characteristic temperatures, J. Non-Cryst. Solids 355 (2009) 2183–2189.
[49] Z.-Z. Yuan, S.-L. Bao, Y. Lu, D.-P. Zhang, L. Yao, A new criterion for evaluating the glass-forming ability of bulk glass forming alloys, J. Alloys Compd. 459 (2008) 251–260.
[50] T.V. Marques, A.A. Cabral, Influence of the heating rates on the correlation between glass-forming ability (GFA) and glass stability (GS) parameters, J. Non-Cryst. Solids 390 (2014) 70–76.
[51] A. Hrubý, Evaluation of glass-forming tendency by means of DTA, Czechoslov. J. Phys. B 22 (1972) 1187–1193.
[52] M. Saad, M. Poulain, Glass forming ability criterion, in: Materials Science Forum, Trans Tech Publ., 1987, pp. 11–18.
[53] I. Donald, The crystallization kinetics of a glass based on the cordierite composition studied by DTA and DSC, J. Mater. Sci. 30 (1995) 904–915.
[54] H.E. Kissinger, Variation of peak temperature with heating rate in differential thermal analysis, J. Res. Natl. Bureau Stand. 57 (1956) 217–221.
[55] T. Ozawa, Kinetics of non-isothermal crystallization, Polymer 12 (1971) 150–158.
[56] T. Ozawa, A new method of analyzing thermogravimetric data, Bull. Chem. Soc. Jpn. 38 (1965) 1881–1886.
[57] J. Augis, J. Bennett, Calculation of the Avrami parameters for heterogeneous solid state reactions using a modification of the Kissinger method, J. Therm. Anal. Calorim. 13 (1978) 283–292.
[58] T.S. Rao, T.L.S. Rao, A. Shaker, K. Venkatraman, Crystallization Kinetics of Amorphous Fe77B16Si5Cr2 Metallic Glass, Tc, 1, T2.
[59] K. Matusita, S. Sakka, Kinetic study of crystallization of glass by differential thermal analysis—criterion on application of Kissinger plot, J. Non-Cryst. Solids 38-39 (1980) 741–746.
[60] L.E. Marques, A.M. Costa, M.C. Crovace, A.C. Rodrigues, A.A. Cabral, Influence of particle size on nonisothermal crystallization in a lithium disilicate glass, J. Am. Ceram. Soc. 98 (2015) 774–780.
[61] X.J. Xu, C.S. Ray, D.E. Day, Nucleation and crystallization of $Na_2O{\cdot}2CaO{\cdot}3SiO_2$ glass by differential thermal analysis, J. Am. Ceram. Soc. 74 (1991) 909–914.
[62] L. Lilensten, Q. Fu, B.R. Wheaton, A.J. Credle, R.L. Stewart, J.T. Kohli, Kinetic study on lithium-aluminosilicate (LAS) glass-ceramics containing MgO and ZnO, Ceram. Int. 40 (2014) 11657–11661.
[63] A. Gaddam, H.R. Fernandes, D.U. Tulyaganov, M.J. Ribeiro, J.M. Ferreira, The roles of P_2O_5 and SiO_2/Li_2O ratio on the network structure and crystallization kinetics of non-stoichiometric lithium disilicate based glasses, J. Non-Cryst. Solids 481 (2018) 512–521.
[64] L. Han, J. Song, Q. Zhang, Z. Luo, A. Lu, Crystallization, structure and characterization of MgO–Al_2O_3–SiO_2–P_2O_5 transparent glass-ceramics with high crystallinity, J. Non-Cryst. Solids 481 (2018) 123–131.
[65] C. Ray, D. Day, Identifying internal and surface crystallization by differential thermal analysis for the glass-to-crystal transformations, Thermochim. Acta 280 (1996) 163–174.
[66] A. Hu, M. Li, D.M. Dali, K. Liang, Crystallization and properties of a spodumene–willemite glass ceramic, Thermochim. Acta 437 (2005) 110–113.
[67] X. Guo, H. Yang, M. Cao, Nucleation and crystallization behavior of Li_2O–Al_2O_3–SiO_2 system glass–ceramic containing little fluorine and no-fluorine, J. Non-Cryst. Solids 351 (2005) 2133–2137.